

# Politecnico di Torino

A dissertation submitted to the graduate faculty

for the degree of

PhD in Electronic Devices



**Graphene Based Nano-Hybrids for High Performance Devices**

Rossella Giardi

Prof. Candido Fabrizio Pirri, Supervisor

Politecnico di Torino, Italy, 2015

Copyright © Rossella Giardi, 2015. All rights reserved.

## DEDICATION

I would like to dedicate this thesis to Bryan and to my family without whose support I would not have been able to complete this work. I would also like to thank my friends and colleagues for their loving guidance and assistance during the writing of this work. To all those that love me...

## ACKNOWLEDGEMENTS

I would like to take this opportunity to express my thanks to those who helped me with various aspects of conducting research and the writing of this thesis. My PhD program was a collaboration between two research centers: IIT CSHR Istituto Italiano di Tecnologia located in Torino (Italy) and the IBM Almaden research center of San Jose (California, USA). The collaboration concerned the study of a novel carbon material: the graphene, the research has been done in the two locations and different applications of a common material were developed. The investigations on printed electronics were pursued in the IIT laboratory while the ones on energy storage devices were pursued at IBM with the support of the Advanced Energy group. I want to thank first and foremost, Dr. Samuele Porro and Dr. Ho-Cheol Kim for their guidance, patience and support throughout this research and the writing of this thesis. Their insights and words of encouragement have often inspired me and renewed my hopes for completing my graduate education. I would also like to thank my managers Prof. Fabrizio Pirri and Dr. Luisa Bozano, that by establish the agreement between Politecnico di Torino and IBM made possible this PhD program. I would additionally like to thank Dr. Marco Sangermano for his guidance throughout the initial stages of the work and Dr. Jeanette Garcia for her inspirational support and teaching style.

## ABSTRACT

Graphene has been drawing much attention in these recent years in the research field, due to its superior material properties and potential for many practical applications. I have been working on synthesizing, characterizing and testing graphene based nano-hybrid materials for electronic devices in the field of flexible printed electronics and energy storage devices. In this dissertation, the preparation, characterization and test of graphene based nano-hybrid materials will be presented and discussed. Starting from investigating environmentally friendly and safer synthesis and reduction techniques to obtain few layer Graphene and reduced Graphene Oxide, to UV-induced photo-polymerization of Reduced Graphene Oxide (rGO)/polymer hybrids and their potential application as a conductive ink for flexible printed electronic devices by tuning the property of polymers. The synthesis and applications of 3D nanostructured rGO/metal oxide hybrids as a high capacity electrode for electrochemical energy storage device such as supercapacitors will be then presented. Intercalation of sodium ( $\text{Na}^+$ ) ions into the electrode will be discussed along with their electrochemical performances. In conclusion, possible future methods to combine the results obtained for a 3D printed all solid state flexible graphene based supercapacitor will be proposed.

## Contents

<b>ACKNOWLEDGEMENTS</b> . . . . .	iii
<b>ABSTRACT</b> . . . . .	iv
<b>Chapter LIST OF FIGURES</b> . . . . .	vii
<b>Chapter LIST OF TABLES</b> . . . . .	xvi
<b>Chapter1. INTRODUCTION</b> . . . . .	1
1.1 Graphene: Material and Properties . . . . .	2
1.2 Flexible Printed Electronics . . . . .	4
1.3 Energy and Power Storage Devices . . . . .	6
<b>Chapter 2. GRAPHENE SYNTHESIS METHODS</b> . . . . .	10
2.1 Synthesis Methods Overview . . . . .	10
2.2 Experimental Session: Synthesis of the Graphene . . . . .	15
2.2.1 Synthesis of Few Layer Graphene in N-Methyl-2-Pyrrolidone . . . . .	18
2.2.2 Synthesis of Few Layer Graphene in Ionic Liquids . . . . .	22
2.3 Conclusion . . . . .	31
<b>Chapter 3. GRAPHENE OXIDE REDUCTION METHODS</b> . . . . .	35
3.1 Reduction Methods Overview . . . . .	35
3.2 Experimental Session: Reduction of the Graphene Oxide . . . . .	37
3.2.1 Sodium Silicate Catalyzed Graphene Oxide Reduction . . . . .	40
3.2.2 UV-light Catalyzed Graphene Oxide Reduction . . . . .	51
3.2.3 Hydrothermal Graphene Oxide Reduction . . . . .	57
3.3 Conclusion . . . . .	62

<b>Chapter 4. GRAPHENE BASED INKS FOR PRINTED ELECTRONIC APPLICATIONS . . . . .</b>	<b>64</b>
4.1 Background . . . . .	64
4.2 Experimental Session: Synthesis of Graphene Oxide/Polymer Composites . . . . .	66
4.2.1 Graphene Oxide/PEGDA UV-Curable Formulations . . . . .	67
4.2.2 Graphene Oxide/PEGDA Inks for Ink Jet Printing Applications . . . . .	70
4.2.3 Preliminary Piezoresistive Measurements . . . . .	80
4.3 Conclusion . . . . .	83
<b>Chapter 5. GRAPHENE BASED ELECTRODES FOR SUPERCAPACITOR APPLICATIONS . . . . .</b>	<b>85</b>
5.1 Background . . . . .	86
5.2 Experimental Session . . . . .	89
5.2.1 Hydrothermal Synthesis of rGO/Molybdenum Dioxide Composites . . . . .	89
5.2.2 Other Graphene Composites . . . . .	110
5.3 Conclusion . . . . .	125
<b>Chapter 6. CONCLUSIONS AND FUTURE WORKS . . . . .</b>	<b>128</b>
<b>APPENDIX A. CHARACTERIZATION METHODS . . . . .</b>	<b>131</b>
A.1 Morphological Characterizations . . . . .	132
A.2 Compositional Characterizations . . . . .	135
A.3 Electrical and Electrochemical Characterizations . . . . .	138
<b>BIBLIOGRAPHY . . . . .</b>	<b>140</b>

## List of Figures

Figure 1.1	Scanning Tunneling Microscope (STM) picture showing the bond's length between two carbon atoms in a graphene sheet. . . . .	2
Figure 1.2	Picture of an electric circuits printed on a flexible substrate. . . . .	4
Figure 1.3	Printed electronics market forecast from NanoMarkets 2012. . . . .	5
Figure 1.4	Rise in energy consumption since the first industrial revolution, 1850-2000, United Nations, 2009. . . . .	6
Figure 1.5	Ragone plot, power density as a function of energy density. . . . .	7
Figure 2.1	Graphic summary of the Graphene synthesis methods. . . . .	11
Figure 2.2	Process steps of the Hummers method. . . . .	13
Figure 2.3	Representation of the intercalation/sonication process used to exfoliate the Graphite. . . . .	16
Figure 2.4	SEM pictures of Expanded Graphite flakes. . . . .	17
Figure 2.5	Raman spectroscopy spectrum of the Expanded Graphite. . . . .	18
Figure 2.6	X-Ray Diffraction spectrum of the Expanded Graphite. . . . .	19
Figure 2.7	Pictures of the Ultrasonication tool used for the exfoliation of the expanded graphite flakes. . . . .	20
Figure 2.8	AFM picture (a) and SEM picture (b) of few layer graphene exfoliated in NMP. . . . .	21
Figure 2.9	AFM height profiles of few layer graphene exfoliated in NMP. . . . .	21
Figure 2.10	Raman spectrum of few layer graphene exfoliated in NMP. . . . .	22
Figure 2.11	Pictures of the chemical representation of BDIM-TFSI (Ionic liquid). . . . .	24

Figure 2.12	Pictures showing the separation of phase and the graphite located at the interface. . . . .	25
Figure 2.13	Pictures of (a) the Ionic liquids and (b) Graphite dispersions in Ionic liquids after sonication process. . . . .	26
Figure 2.14	SEM pictures of the few layer graphene obtained from the exfoliation in ionic liquid. . . . .	27
Figure 2.15	Optical microscope image on 300 nm SiO <sub>2</sub> wafer. . . . .	28
Figure 2.16	AFM Height scan showing the few layer graphene obtained by ionic liquid exfoliation. . . . .	29
Figure 2.17	AFM profile measurement showing the different thickness of the few layer graphene flakes. . . . .	29
Figure 2.18	Raman spectroscopy spectrum showing the shift of the 2D peak after the exfoliation process of the Expanded Graphite (green) 2717 cm <sup>-1</sup> and two samples (blue and red) 2703 and 2675 cm <sup>-1</sup> . . . . .	30
Figure 2.19	Raman spectroscopy spectrum of the Expanded Graphite after the exfoliation process. . . . .	31
Figure 2.20	Raman Spectrum of Graphene and Graphene Layers A. C. Ferrari, J. C. Meyer, V. Scardaci, C. Casiraghi, M. Lazzeri, F. Mauri, S. Piscanec, D. Jiang, K. S. Novoselov, S. Roth, and A. K. Geim, Phys. Rev. Lett., 2007, 97, 187401. . . . .	32
Figure 2.21	Raman spectroscopy spectrum of the 2D peak of two Expanded Graphite flakes with different thickness. . . . .	33
Figure 2.22	Coin cell on the left used for impedance measurements and impedance setup. . . . .	33
Figure 2.23	Impedance graphs of ionic liquid BDMI-TFSI (pink), BDMI-TFSI and expanded graphite (red) and BDMI-TFSI and commercial graphene (green). . . . .	34



Figure 3.1	Optical picture (a), Raman spectrum (b) and SEM picture (c) of commercial graphene oxide deposited on a 300 nm silica oxide wafer. . . . .	38
Figure 3.2	XRD data of commercial graphene oxide. . . . .	39
Figure 3.3	XPS data of commercial graphene oxide. . . . .	39
Figure 3.4	Sodium silicate chemical reaction formation and graphic representation of the structure of the structure of the silica gel. . . . .	40
Figure 3.5	Table reporting the parameters of the samples of graphene oxide in sodium silicate water solution prepared. . . . .	42
Figure 3.6	Pictures showing the different colors of the samples prepared with different concentration of sodium silicate and heated for different period of time. . . . .	42
Figure 3.7	FE-SEM pictures of reduced graphene oxide after temperature treatment in sodium silicate solution. . . . .	44
Figure 3.8	Picture of a freestanding rGO easily manageable flexible paper on an alumina filter for vacuum filtration. . . . .	45
Figure 3.9	FE-SEM pictures of the top view and cross section of the layered reduced graphene paper obtained after vacuum filtration. . . . .	45
Figure 3.10	X-Ray Diffraction spectra of expanded graphite (blue), graphene oxide (pink) and reduced graphene oxide with sodium silicate (green). . . . .	46
Figure 3.11	X-Ray Photoelectron Spectroscopy spectra of a) Graphene oxide and b) reduced graphene oxide. . . . .	47
Figure 3.12	Pictures of the dispersions of GO in water with 1M of Na <sub>2</sub> SiO <sub>3</sub> and 1M NaOH before and after the reduction reaction. . . . .	47
Figure 3.13	Pictures of the dispersions of GO in water compared to dispersion with 1M of Na <sub>2</sub> SiO <sub>3</sub> and 1M NaOH after thermal treatment. . . . .	48
Figure 3.14	Pictures of the dispersions of GO in water and GO/1M of Na <sub>2</sub> SiO <sub>3</sub> , GO/8M NaOH and GO/1M NaOH after the reduction reaction. . . . .	49

Figure 3.15	X-Ray Photoelectron Spectroscopy spectra of a) Graphene oxide and b) reduced graphene oxide with 1M of Na <sub>2</sub> SiO <sub>3</sub> , c) 1M NaOH and d)8M NaOH. . . . .	50
Figure 3.16	Darocur 1173 . . . . .	53
Figure 3.17	Image showing inkjet print head, printing on a glass slide. . . . .	53
Figure 3.18	Hg-lamp, UV-light with intensity 55 mW/cm <sup>2</sup> . . . . .	54
Figure 3.19	Image showing inkjet printed test tracks of the GO ink on a microscope glass, after UV irradiation. . . . .	54
Figure 3.20	XPS spectra of pristine GO (a) and a sample irradiated for 2 min with UV light (b) . . . . .	55
Figure 3.21	Analysis of XPS C1s peak deconvolution: height (a) and area (b) ratios of C=O to C–C contributions plus height (c) and area (d) ratios of O–C=O to C–C contributions. . . . .	56
Figure 3.22	Picture of the Teflon-lined autoclave used for the hydrothermal synthesis. . . . .	57
Figure 3.23	Photograph of the GO/DI water dispersion (a); reduced graphene oxide hydrogel obtained from the hydrothermal synthesis (b) and FESEM showing its porous structure (c). . . . .	58
Figure 3.24	Picture of the hydrogels with a spatula on top. . . . .	58
Figure 3.25	XPS spectra of a) Graphene oxide and b) reduced graphene oxide after hydrothermal synthesis . . . . .	60
Figure 3.26	X-Ray Diffraction spectra of expanded graphite (blue), graphene oxide (pink) and reduced graphene oxide with hydrothermal synthesis (red). . . . .	61
Figure 3.27	Raman spectroscopy data comparing the commercial graphene oxide (blue line) and reduced graphene oxide (red line). . . . .	62
Figure 3.28	Thermo gravimetric analysis of the rGO hydrogel formed with the hydrothermal synthesis. . . . .	63
Figure 4.1	Photo-polymerization steps process. . . . .	68
Figure 4.2	poly ethylene glycol diacrylate with Mw = 575 g mol <sup>-2</sup> . . . . .	68

Figure 4.3	Four-probe measurements of surface resistance . . . . .	69
Figure 4.4	SEM image showing the top surface microstructure of the thick rGO/PEGDA film after the UV-irradiation. . . . .	70
Figure 4.5	SEM image showing the cross-section microstructure of the thick rGO/PEGDA film after the UV-irradiation. . . . .	71
Figure 4.6	Ink Jet printer used for the experiments, with parameters fluid viscosity: 1-20 cP, drop volume: 10 pl 1 nl, nozzle diameter: 20-100 $\mu\text{m}$ , drop velocity: 3 10 $\text{ms}^{-1}$ . . . . .	71
Figure 4.7	Ink Jet printer tesion signal applied to the piezoelectric coponent for the control of the drop ejection. . . . .	72
Figure 4.8	Ink Jet printer mechanism process. . . . .	72
Figure 4.9	GO/PEGDA/water ink (a), InkJet nozzle printing GO/PEGDA/water ink (b), and the two-point micro-contact setup for IV measurements used for inkjet printed GO thin films (c) . . . . .	74
Figure 4.10	Structural inspection of RGO/PEGDA inkjet-printed tracks on a glass slide after UV irradiation: top-view optical microscopy image of a 500 $\mu\text{m}$ wide track (a) and a profilometry scan showing a thickness of about 10 $\mu\text{m}$ (b) . . . . .	74
Figure 4.11	SEM image showing the microstructure of an inkjet printed track of PEGDA/GO track. The inset shows a low-resolution image of the printed track . . . . .	75
Figure 4.12	Raw IV characteristics of pure PEGDA and GO thick films (TF), and GO inkjet printed thin film. . . . .	76
Figure 4.13	Resistivity of GO inkjet printed and thick film (TF) samples, as computed from linear fit to IV curves, as a function of the sample thickness. Error bars are shown on experimental data points. The series refer to the inkjet printed tracks with single (blue solid arrow) and multiple (green dashed arrow) passes . . . . .	77

Figure 4.14	Analysis of the coefficients of dispersion as a function of the film thickness: GO are the ink jet printed tracks, GO TF are the thick film of the GO/PEGDA compound and the PEGDA the pure matrix. . . . .	78
Figure 4.15	Real-time variation of PEGDA/GO resistance during UV irradiation, starting from as-printed non-polymerized material (time = 0), for three different UV light power densities . . . . .	79
Figure 4.16	Real-time variation of sample resistance during UV irradiation for pure PEGDA polymeric matrix (upper red line) and the PEGDA/GO composite (lower blue line), starting from as-printed non-polymerized material (time = 0) . . . . .	80
Figure 4.17	Piezoresistive samples preparation method. . . . .	81
Figure 4.18	Piezo resistive measurements, (a) PEGDA 5% rGO, (b) PEGDA 10% rGO and (c) BEMA 5% rGO. . . . .	83
Figure 4.19	Piezo resistive measurements, (a) pure matrices PEGDA and BEMA and (b) PDMS with GO and rGO. . . . .	84
Figure 5.1	Supercapacitors types scheme. . . . .	87
Figure 5.2	EDLC charge/discharge schematic representation. . . . .	88
Figure 5.3	FESEM pictures of (a) RGO and (b) RGO/MoO <sub>2</sub> composite synthesized by hydrothermal process. . . . .	92
Figure 5.4	FESEM pictures of RGO/MoO <sub>2</sub> composite synthesized by hydrothermal process, showing the graphene porous structure and the presence of MoO <sub>2</sub> nanoparticles decoration. . . . .	93
Figure 5.5	Bright-Field TEM images of MoO <sub>2</sub> nanoparticles (a) and HRTEM magnification of crystalline structure (b). . . . .	94
Figure 5.6	Electron Energy loss spectra performed on the nanoparticles. . . . .	95
Figure 5.7	XPS survey spectra of the rGO/MoO <sub>2</sub> composite. . . . .	96
Figure 5.8	XPS deconvolution spectra of (a) the C1s peak and (b) the Mo 3d high-resolution scans. . . . .	97

Figure 5.9	XRD spectra of MoO <sub>2</sub> nanoparticles. . . . .	98
Figure 5.10	Micro-Raman spectra of RGO, MoO <sub>2</sub> nanoparticles and the RGO/MoO <sub>2</sub> composite. . . . .	98
Figure 5.11	TGA of RGO (green), MoO <sub>2</sub> nanoparticles (blue) and RGO/MoO <sub>2</sub> composite (red). . . . .	99
Figure 5.12	XRD spectra of MoO <sub>2</sub> nanoparticles before (blue graph) and after the TGA (red graph). . . . .	99
Figure 5.13	Photograph of the RGO/MoO <sub>2</sub> composite before (a) and after (b) annealing at 325°C. . . . .	100
Figure 5.14	Photograph of the two-electrode cell used for the electrochemical characterization. . . . .	101
Figure 5.15	GCD profiles of RGO/MoO <sub>2</sub> , KJ Black and RGO electrodes recorded in the range of -1.5 V to 1.5 V, at a current of 0.5 mA at 1 mAh. . . . .	102
Figure 5.16	Galvanostatic discharges of RGO/MoO <sub>2</sub> and RGO electrodes at a current of 0.5 mA at 1 mAh, first four cycles. . . . .	103
Figure 5.17	First CV cycle of RGO/MoO <sub>2</sub> electrodes recorded in the range of -1.5V to 1.5V, with a scan rate of 0.5 mV/s. . . . .	104
Figure 5.18	CV profiles of the current density versus voltage of RGO/MoO <sub>2</sub> electrodes recorded in the range -1.5V to 1.5V, with a scan rate of 0.5, 2 and 5 mV/s. . . . .	105
Figure 5.19	CV profiles of the current density of RGO (red line) and RGO/MoO <sub>2</sub> (blue line) electrodes versus voltage in the range -1.5V to 1.5V, with a scan rate of 0.5,mV/s. . . . .	106
Figure 5.20	FESEM picture of the RGO/MoO <sub>2</sub> electrodes after discharge (a), EDS mapping of Na k and Mo L edges (b) and XRD spectra before and after (blue) discharge process (c). . . . .	108
Figure 5.21	EIS after 5 GCD cycle of RGO (green line) and RGO/MoO <sub>2</sub> (blue line) electrodes. . . . .	109

Figure 5.22	Equivalent electric circuit of a double-layer capacitor used for RGO and KJB electrodes (a) and of a pseudocapacitor used for RGO/MoO <sub>2</sub> electrode (b). . . . .	109
Figure 5.23	SEM picture at 6.5 kV of rGO/TiO <sub>2</sub> composites with different ratio of graphene to TiO <sub>2</sub> (a) 5:1 (b) 1:1 (c) 1:3 and (d) 1:4. . . . .	116
Figure 5.24	Raman spectra of rGO/TiO <sub>2</sub> composite (a) and high-resolution scan on TiO <sub>2</sub> peaks (b). . . . .	117
Figure 5.25	Cyclic voltammetry of the composite rGO/TiO <sub>2</sub> with the ratio 1:1 at 0.5, 2 and 5 mV/s in a voltage range of 1.5 to -1.5 V. . . . .	117
Figure 5.26	Cyclic voltammetry of the composite rGO/TiO <sub>2</sub> with the ratio 1:3 at 0.5, 2 and 5 mV/s in a voltage range of 1.5 to -1.5 V. . . . .	118
Figure 5.27	EIS spectra of RGO/TiO <sub>2</sub> 1:3 (purple line) and RGO/TiO <sub>2</sub> 1:1 (green line). . . . .	118
Figure 5.28	Photos and SEM pictures of 10% and 50% expanded graphite respect to the total amount of carbon material. . . . .	119
Figure 5.29	SEM pictures at different magnification of 10% and 50% expanded graphite respect to the total amount of carbon material. . . . .	120
Figure 5.30	SEM pictures at different magnification of 30% expanded graphite respect to the total amount of carbon material. . . . .	121
Figure 5.31	Cyclic voltammetry of the composite 30% expanded graphite/rGO at 0.5, 2 and 5 mV/s in a voltage range of 1.5 to -1.5 V. . . . .	121
Figure 5.32	Sodium silicate gel chemical structure after gelation. . . . .	123
Figure 5.33	Sodium silicate gel conditions. . . . .	123
Figure 5.34	Sodium silicate gel. . . . .	124
Figure 5.35	Sodium silicate gel with graphene oxide as a filler. . . . .	124
Figure 5.36	Electrode assembling process scheme. . . . .	125
Figure 5.37	Pictures of GO/sodium silicate electrodes gel on metal grid after aging and washing processes. . . . .	125

Figure 5.38 Cyclic voltammetry of sodium silicate gel electrodes at 50 and 100 mV/s  
in a voltage window of -0.5V to +0.5V. . . . . 126

Figure 5.39 Cyclic voltammetry of RGO/sodium silicate gel electrodes at 50 and  
100 mV/s in a voltage window of -0.5V to +0.5V. . . . . 127

## List of Tables

Table 1.1	Comparison of tensile strength, thermal and electrical conductivity values for Graphene, Carbon Nanotubes (CNTs), A36 steel, High Density Polyethylene and rubber. . . . .	3
Table 3.1	Survey atomic percentage of C 1s and Na KLL. . . . .	45
Table 3.2	Samples concentrations, temperature and time of the reduction process.	47
Table 3.3	Samples concentrations, temperature and time of the reduction process.	48
Table 3.4	Ratio C/O of carbonyl and carboxyl group of GO, GO/8M NaOH, GO/1M of Na <sub>2</sub> SiO <sub>3</sub> and GO/1M NaOH samples. . . . .	49
Table 3.5	XPS peak area C/O ratios for different functional groups of GO and rGO	60
Table 5.1	Specific capacitances of RGO and RGO/MoO <sub>2</sub> electrodes at 0.5, 2 and 5 mV/s scan rates calculated from CV measurements. . . . .	104
Table 5.2	Comparison of ESR values for RGO, KJB and RGO/MoO <sub>2</sub> electrodes calculated from GCD measurements (IR drop of the discharge using CC curves) and from zFit software fitting of EIS data. . . . .	107
Table 5.3	Specific capacitances of RGO and RGO/TiO <sub>2</sub> (1:1) electrodes at 0.5, 2 and 5 mV/s scan rates calculated from CV measurements. . . . .	113
Table 5.4	Specific capacitances of RGO and 30% expanded graphite/rGO electrodes at 0.5, 2 and 5 mV/s scan rates calculated from CV measurements.	115



## Chapter1. INTRODUCTION

In these recent years we are witnessing an increasing demand for electronic devices production characterized by high demanding criteria such as low manufacturing cost, high endurance, environmentally sustainable production methods, recyclability, low energy consumption, and high efficiency. The investigation of novel materials for electronic devices and energy storage devices is a continuously growing research field.

In this dissertation, the results of my PhD investigations on novel composite materials for flexible printed electronics and high performance energy storage device applications will be discussed. The research was directed towards the synthesis and characterization of novel carbon based composite materials and their assessment as candidates for different applications. The goal and motivations were driven by keeping in mind the important aspects of environmentally friendly, non toxicity, safety and low cost of materials and processes, with an eye the possible scaling up constraints for a final device.

Readily available and low-cost resources were employed in order to keep the production cost as low as possible and carbon based materials together with non toxic metal oxides and polymers are at the center of the study because are considered environmentally friendly materials especially if used with water based solvents. For the study on novel electrode materials for energy storage devices, large attention has been put in finding a good hosting material for sodium ions, used as intercalating material, that are considered safer and cheaper because more abundant on earth respect for examples to the lithium ions. In terms of cost, abundance and electronic conductivity, the carbon based material results to be the perfect choice to be employed in electronic devices and the focus on a particular carbon material has grown in recent years, due to its powerful properties and the large range of applications in which it can be used: the graphene.

## 1.1 Graphene: Material and Properties

Graphene was isolated for the first time in 2004 in the laboratory of the group of Prof. Novoselov and Prof. Geim in Manchester (UK), to whom the Nobel prize was then assigned in 2010 for their study on the structure and properties of graphene (1). Lots of effort were put into the investigation of different routes for the synthesis of the graphene, the study of its properties (2)-(8). In recent years the interest in the graphene has grown in both academic and industry fields due to its great and diverse properties. Graphene properties have been deeply investigated showing very high performances and due to its unique chemical, electrical and physical properties, the graphene has been the object of many studies for many different applications.

The graphene is a monolayer of carbon atoms organized in an hexagonal structure with the carbon bond length of about  $1.42 \text{ \AA}$ , as shown in the scanning tunneling microscope picture, in Figure 1.1. The carbon-carbon chemical bonds have a hybridization of  $sp^2$ . Due to hy-

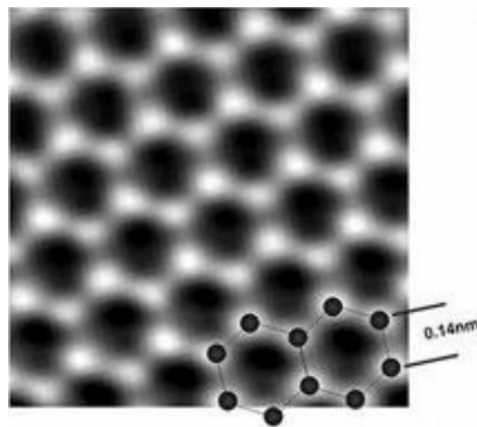


Figure 1.1 Scanning Tunneling Microscope (STM) picture showing the bond's length between two carbon atoms in a graphene sheet.

bridized orbitals generated by the superimposition of  $2s$  with  $2p_x$  and  $2p_y$  orbitals, the planar orbitals form the energetically stable and localized sigma bond and the three near carbon atoms in the lattice are responsible for most of the binding energy and for the elastic properties of the graphene sheet. The remaining  $2p_z$  orbitals present the  $\pi$  symmetric orientation and the overlap of these orbitals of the near atoms play an important role in the electric properties of

the graphene sheets (9).

The graphene is among the thinnest materials known to man, the lightest, 1  $m^2$  is about 0.77 mg and also the strongest compounds discovered, with a tensile strength of 150 MPa and a Young's modulus higher than 0.5-1 TPa (10). In Table 1.1 are reported tensile strength, thermal and electrical conductivity of the Graphene compared with Carbon Nanotubes (CNTs), A36 steel, high density polyethylene and rubber, showing how the properties of the graphene are superior to the other materials that make it an ideal candidate for a very large number of applications. The graphene is also good thermal and electric conductor with a theoretical

Table 1.1 Comparison of tensile strength, thermal and electrical conductivity values for Graphene, Carbon Nanotubes (CNTs), A36 steel, High Density Polyethylene and rubber.

Materials	Tensile Strength	Thermal Cond. (W/m k)	Electrical Cond. (S/m)
Graphene	130 GPa	4.84-5.30x10 <sup>3</sup>	7200
CNTs <sub>3</sub>	60-150 GPa	3500	3000-4000
A36 steel	400 MPa	5-6	1.35x10 <sup>6</sup>
HDPE	18-20 MPa	0.46-0.52	Insulator
Rubber	20-30 MPa	0.13-0.14	Insulator

carrier mobility of 15000  $cm^2 V^{-1} s^{-1}$  (11) and resistivity of  $10^{-6}$  ohm cm, that combined with the Johnson noise, makes the graphene a perfect candidate as a channel material for field-effect transistors (FET) (12), (13); it is also transparent to almost 97% of optical transmittance (19) with almost 2.2 kohm/sq sheet resistance, that is considered ideal for example for transparent conductive electrodes. Its chemical stability and high surface area, of about theoretically 2700  $m^2 g^{-1}$  make the graphene ideal for energy storage applications. The graphene can also be functionalized, for example biosensors that use DNA functionalized graphene capable of detecting external DNA genes associated with diseases (14), gas sensors based on graphene (15) and biological sensors (16)-(18) have also been reported in literature.

The high electrical conductivity and optical transparency make graphene a good candidate material for transparent conducting electrodes for several applications like organic photovoltaic cells, organic light emitting diodes and touch screens (11). For its properties of high strength, good conductivity, and high thermal stability graphene is also a good candidate for formula-

tion of graphene-polymer composites (20)-(22). The association of graphene with nanoparticles can have applications regarding catalysis and electrochemical sensors; in addition graphene-semiconductor materials composites can be employed in energy field as solar cells, energy storage materials, (23), chemical and electrocatalysis (24).

## 1.2 Flexible Printed Electronics

Flexible printed electronics is a sector that has been growing in the last years reaching a wide range of applications in different areas, such as building materials or textiles, by creating smart buildings that adjust their own environments for optimal energy consumption or clothing that adapts to the wearers needs and which monitors physiology. Printed electronics uses existing graphics publishing industry manufacturing capabilities to produce circuitry at high speeds and at reduced costs (Figure 1.2). Electronics can be printed with several methods,

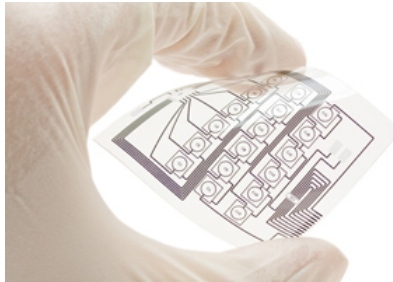
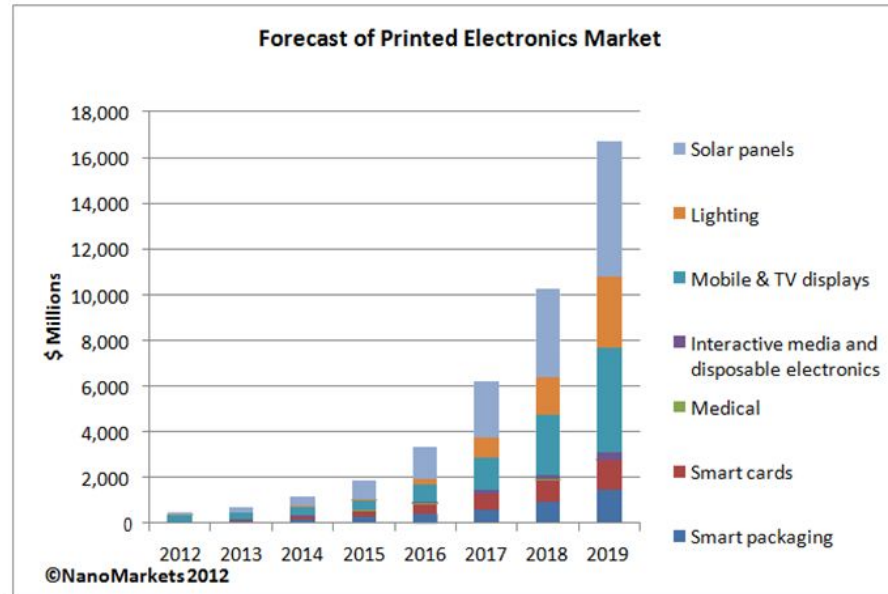


Figure 1.2 Picture of an electric circuits printed on a flexible substrate.

including screen, offset, gravure, flexo or ink jet printing, with feature sizes in the 10-20 micron range that allowed to emerge a new industry: the flexible printed electronics.

This industry combined the breadth of the printing industry with smart electronics and it has provided new market opportunities. A reasonable estimate is from NanoMarkets, which forecasts a \$1.15B printed electronics market in 2014 growing to \$16.7B in 2019 as reported in Figure 1.3, where the analysts acknowledge that emerging flexible printed electronic applications are going to be in sensors, power, communications, and lighting fields.

Hybrid devices fall in between all silicon devices and fully printed ones, and are naturally



Printed Electronics Market Forecast from NanoMarkets

Figure 1.3 Printed electronics market forecast from NanoMarkets 2012.

bridged between the two sectors. At the Semicon West 2013 in San Francisco, companies reported on progress in hybrid devices, materials and processing technologies for flexible, conformable electronics. They described near-to-market applications including wearable biomedical sensors and imagers, displays, consumer packaging, and toxic and structural sensors, opening the large possibility to smart packaging and embedded electronics. Electronic supply chain companies are already testing this with PET and PEN substrate films (DuPont Teijin Films in Richmond, Virginia), enabling new aspects of the flexible signage, lighting, photovoltaic, and displays markets (25).

Inkjet printing is one of the most promising manufacturing techniques, which can be used to deposit polymers on a variety of substrates (26). Several reviews dealing with new applications of inkjet printing technology are now available (27), (28). Several materials have been tested for use as conductive inks (29), reporting different drawbacks. For instance, conductive polymers presented the disadvantage of relatively low conductivity (30), while metal nanoparticles (NPs) based inks need to be sintered at temperatures generally too high for application on most flexible substrates (31), (32). As an alternative, carbon-based materials can be good candidates to

be fillers for conductive inks, due to their low cost and good electrical conductivity without the need of temperature treatments. This has already been demonstrated for carbon nanotubes printed thin films (140), graphene bi- and tri-layers used as protective coatings against oxidation on copper NPs-based inks (141), and for graphene/water suspensions (35).

### 1.3 Energy and Power Storage Devices

In recent years an increasing demand for energy availability and power consumption has been raised worldwide in many areas of the everyday life, with an acceleration of global primary energy consumption despite stagnant economic growth (38) (Figure 1.4). These data are

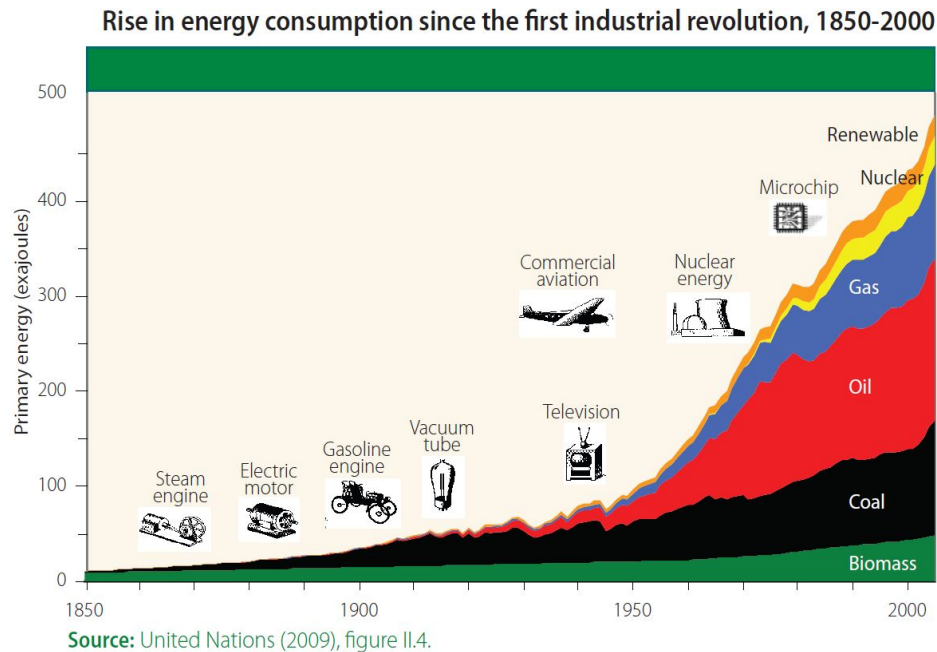


Figure 1.4 Rise in energy consumption since the first industrial revolution, 1850-2000, United Nations, 2009.

predicted to keep rising over the next decades, particularly in nations outside the Organization for Economic Co-operation and Development (OECD) (39). In order to engage this growing demand, the necessity of finding new and alternative resources, and to increase the efficiency and performance of devices, is becoming increasingly urgent. This is expected to be crucial for applications such as memory back-up devices where power is needed for very short period,

portable and personal electronics where battery systems need improvement for high-power pulsed currents, renewable energy devices in order to improve their lifetime, or electric and hybrid vehicles (156). In particular, although great improvements were recently achieved in the field of electric cars, the decisive goal of fabricating reliable and efficient long-life batteries and supercapacitors has yet to be achieved (41).

Supercapacitors are electrochemical power storage devices that can find a practical application in support of the main battery of a car in specific conditions, such as acceleration, starting and stopping, and to supply power to accessories as for instance the rear mirrors movement. The main advantages of supercapacitors towards batteries are their higher power density values (up to  $10 \text{ kW kg}^{-1}$ ), their much longer cycle life ( $10^5$  versus 500-1000), and a fast charge/discharge rate that allows them to supply power much quicker than batteries, which are not able to provide instantaneous power because their chemistry is much slower. On the negative side, supercapacitors show much lower energy densities ( $5 \text{ Wh kg}^{-1}$  versus  $100\text{-}250 \text{ Wh kg}^{-1}$  for batteries), therefore it is usually still necessary to couple them with batteries in order to supply energy for long periods of time (42).

In Figure 1.5 is reported the Ragone plot, that shows how the different energy storage devices are distributed in function of their energy density and power density. The fabrication of

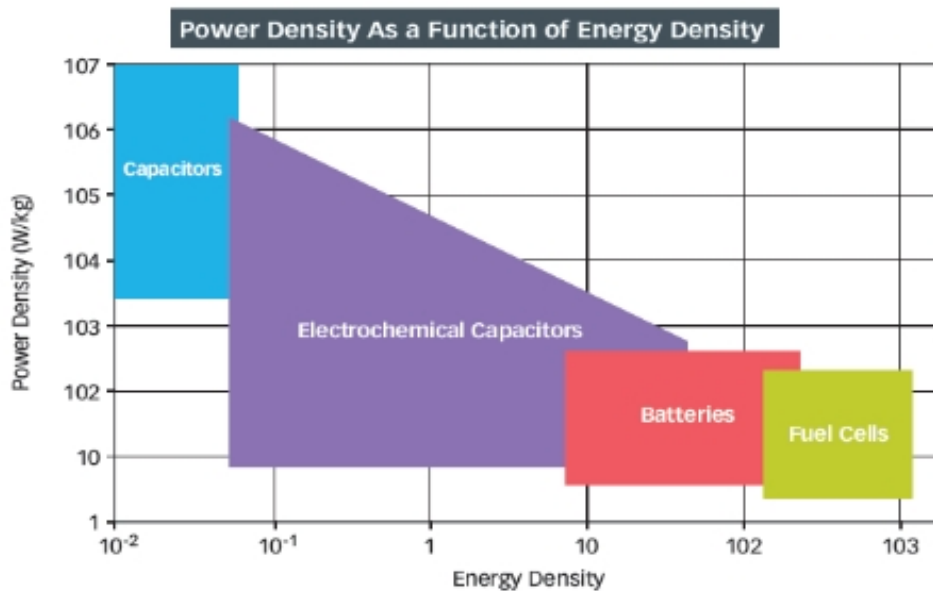


Figure 1.5 Ragone plot, power density as a function of energy density.

nanostructured electrodes is expected to improve the performances of the supercapacitors, in particular with the aim of increasing their energy density without losing the high power density. In fact, supercapacitors are able to store power due to a separation of charges exploiting fast reactions that take place at the interface between electrode and electrolyte, therefore they can benefit from the use of materials with a high surface area. In addition, the research on materials and fabrication technologies should point in the direction of reducing the cost of the electrolyte, while keeping a good operating window and ionic conductivity, adopting scalable fabrication methods, and improving the safety of the cell chemistry, for instance by using aqueous-based electrolytes.

All the experiments presented in this dissertation, have the graphene as common material. The goals of these investigations were set respecting the purpose of using environmentally friendly, non-toxic, safe and low cost materials and processes. Graphene synthesis techniques will be presented in chapter 2, starting from a brief review on the existing graphene synthesis methods. The discussion will then continue with two of the many synthesis approaches that were studied during this work and that are reported in detail. Reduction methods for graphene oxide will be presented in chapter 3, after an initial analysis of the existing reduction methods for the graphene oxide. The most successful techniques investigated for the reduction of the graphene oxide will be reported and discussed in detail.

Both synthesis and reduction techniques have been pursued by following environmentally friendly methods considered safer compared to the most diffused methods. Because of its high specific surface area, good chemical stability, electrical and thermal conductivity, and high charge carrier mobility ( $20 \text{ m}^2 \text{ V}^{-1} \text{ s}^{-1}$ ) (36), (37), graphene is actually the most suitable candidate to be dispersed in photo-curable formulations to obtain UV-cured conductive inks. In chapter 4 novel uses of the graphene as filler in UV curable polymeric matrices will be presented together with the feasibility of using these composites to formulate inks for inkjet printing applications, in order to achieve an enhancement of the conductivity of the printed track due to the contribution of the graphene filler and the possible application of these non toxic and water based conductive inks in flexible printed electronics.



In the last chapter of this dissertation will be presented another kind of graphene application in the energy storage field, in particular the synthesis of graphene/metal oxide nanocomposite through the use of environmental friendly processes and non toxic materials is going to be presented together with the characterizations of these material as electrode material for supercapacitors applications. Sodium ions considered safe, cheap and more environmentally friendly were employed as intercalating material in 3D graphene based porous nanostructures obtained through the use of hydrothermal synthesis. An extensive analysis of the material properties and its electrochemical behavior as electrode material for hybrid supercapacitor is also presented. The conclusions of this work will be summarized in chapter 6 and future investigations are also discussed, about possibly involving the combination of the two applications presented in chapter 4 and 5, for the fabrication of a 3D printed high surface area graphene based supercapacitor. The appendix contains general descriptions and some specifications of all the characterizations that have been employed for the study of the materials and the devices. The characterizations are divided in morphological, compositional and electrical/electrochemical groups.

## Chapter2. GRAPHENE SYNTHESIS METHODS

The graphene synthesis topic has been really well investigated in the last decade and most efforts have been directed towards finding solutions that could lead to large scale production of graphene at a low cost keeping the processes as much more environmentally friendly as possible. In this chapter the most common methods for the production of the graphene are briefly reviewed and subsequently, two of the several top-down synthesis techniques involving direct exfoliation of graphite are reported in detail.

### 2.1 Synthesis Methods Overview

The solution to problems like the limited graphene mass-production and poor reproducibility of device performances, is very important in order to push the graphene-based technology into commercialization of products. Several techniques have been investigated for the synthesis of the graphene and one of the first methods was the mechanical exfoliation, obtained for the first time by Novoselov group (1). The mechanical exfoliation together with the chemical and thermal exfoliation (43) and chemical vapor deposition (44) are considered the most used techniques for the synthesis of the graphene. A scheme summarizing all the different approaches for the synthesis of the graphene is reported in Figure 2.1, showing that basically there are only two possible different approaches: top-down and bottom-up.

Bottom-up techniques, for example, are chemical vapor deposition (CVD) (45), (46) and epitaxial growth (47) processes. Thermal CVD is usually applied for the growth of graphene on transition metals like copper, nickel, iridium and ruthenium (45),(48)-(50). A monolayer of graphene can be grown on different substrates by a simple reaction of dissociation of gases in

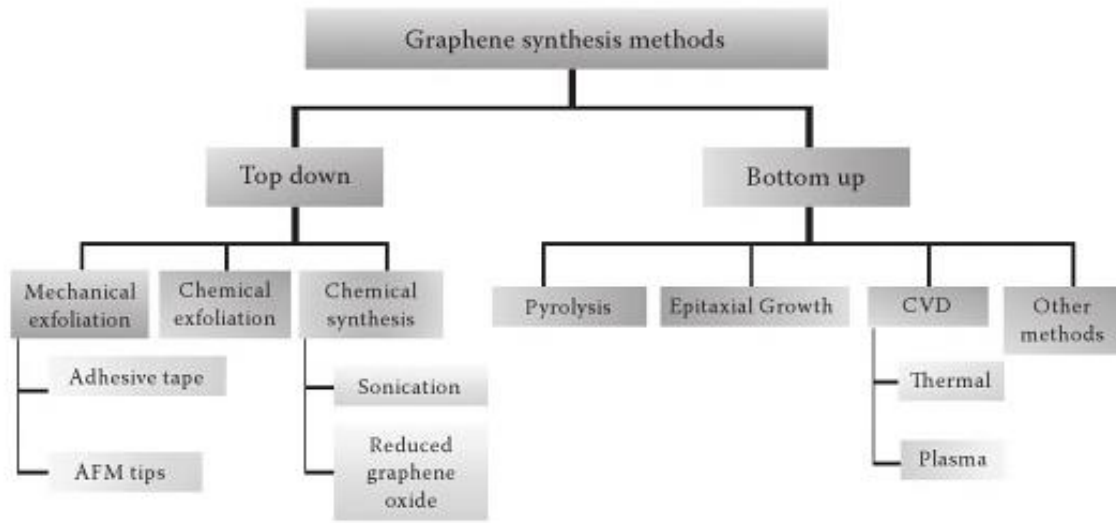


Figure 2.1 Graphic summary of the Graphene synthesis methods.

a reaction chamber and the deposition of the carbon atoms on the heated substrate. Different wafer sizes can be used, reaching a very high quality of the material with a very low amount of defects. On the down side, these kind of processes are usually very slow and they require subsequent steps, as for example the removal of graphene from the surface of the wafer and transfer it to another substrate, increasing the cost of the process due to the sacrificial substrates (ex. copper). In the end, it can be hardly scalable into a production line and the gases produced are toxic.

A completely different approach for the synthesis of the graphene consists in top-down techniques, that involve the production of the graphene starting from the bulk graphite. In fact, the graphite is formed by a stack of many layers (graphene) bound together in the z plane by Van der Waals forces that are less strong compared to the covalent bonds present in the xy plane and for this reasons are easier to brake. The distance between the layers is about 3.34 Å, that gives for 1 mm thick graphite  $3 \times 10^6$  graphene layers.

The mechanical exfoliation method consists in the use of an adhesive scotch tape to generate longitudinal or transverse stress on the surface of a layered structure material, generally high ordered pyrolytic graphite, in order to break the Van der Waals forces that keeps the layers

together slicing them down. The force required to break the bond has been estimated to be  $300 \text{ nN}/\mu\text{m}^2$  (51). The mechanical exfoliation is an easy technique that gives more control on the number of the layers obtained with respect to other synthesis methods, but on the down side, is not scalable because it is not possible to obtain very large quantities of material and the results are not always reproducible. In order to overcome the problems of mechanical exfoliation, both chemical and physical methods have been proposed for the preparation of graphene sheets (8), including production from colloidal suspensions and electrochemical methods (52). The obtainment of graphene sheets from colloidal suspensions is considered advantageous because of its simplicity and its high yield, and because the product obtained it is ready to be used for a wide range of applications.

There are two different processes in order to obtain graphene sheets from colloidal suspensions: by chemical modification of graphite through an oxidation step and then reduction after the exfoliation process (53) and by direct exfoliation in suitable organic solvents without chemical modification (54) or surfactants (55). Unlike direct exfoliation, chemical modification results in considerable destruction of graphene atomic structure, that compromises its unique properties. The most employed chemical exfoliation method for the synthesis of the graphene is the so called Hummer's method (56), that consists in the oxidation of the graphite and the subsequent exfoliation of it in several solvents. The steps are shown in Figure 2.2. This approach involves the oxidation of the graphite with the use of strong acids as sulfuric acid, sodium nitride and potassium permanganate in order to obtain a more soluble material in polar solvents by introducing oxygen functional groups in the graphitic layers that will help the subsequent exfoliation step. The oxidation process, in fact, leads to an increase of the spacing between the layers with the introduction of oxygen functional groups as the carboxyl, carbonyl or hydroxide groups, that can lead, after only one hour of oxidation, from  $3.34 \text{ \AA}$  to  $5.62 \text{ \AA}$  of interlayer distance. After that, the exfoliation step can be performed in several different solvents with the use of ultrasonication equipments.

The chemical exfoliation process has a higher efficiency compared to other techniques but at the same time has also several down sides. Starting from the fact that it is not an environmentally friendly technique, because it involves highly corrosive materials involved in the oxidation

process and from the functional side this method introduces many defects in the structure of the graphene, producing an actual graphene oxide which properties are really different from the ones discussed in the introduction. For this reasons, after every oxidation step, a reduction one must follow in order to remove most of the functional groups from the surfaces and the edges of the graphene oxide sheets. The reduction method employed in the Hummer's method involves the use of a strong and toxic reducing agent: the hydrazine hydrate, combined with surfactants in order to maintain the resulting dispersion stable in solution avoiding re-aggregations and precipitation of particles.

So far the methods just described are considered the ones with the highest yield but at the



Figure 2.2 Process steps of the Hummers method.

same time the quality of the product material is not very encouraging, because of the defects introduced in the atomic structure and the functional group deriving from the oxidation process. For these reasons, other chemical methods have been investigated, like the intercalation of large alkali ions in the graphite layers and the subsequent exfoliation throughout ultrasonication treatments in solution (8), (54) and (58). The alkali metals are materials that can easily form graphite-intercalated structures thanks to their smaller radius compared to the interlayer spacing of the graphite. An example was shown using potassium ions (59) forming a  $KC_8$  intercalated compound. By dispersing the compound into aqueous solutions of ethanol, an exothermic reaction was generated, that lead to hydrogen generation that it is the agent that helps the exfoliation of the graphite. This kind of reaction can be unfortunately unsafe if not handled with precaution and for scalable production, ice must be kept around the reaction bath in order to control the effects and dissipate the heat. Other approaches for the synthesis of the graphene that have been also reported in these last years include microwave

assisted exfoliation (60), unzipping carbon nanotube (61), plasma-assisted etching of graphite (62) and electrochemical exfoliation (52). All the techniques presented so far have different advantages and disadvantages. In fact, CVD growth can give large surface area coating but with slow processes and high cost, mechanical exfoliation gives a better control on the number of layers produced for every sample but it is not an easily scalable technique. The chemical route seems the most favorable because it can lead to higher yields and scalability, also if there is not a precise control in the thickness of the resulting graphene flakes and, especially with the Hummer's method, an oxidative process is involved with a subsequent reduction step, that severely affects the properties of the final product, like its electrical conductivity. The reduced graphene oxide in fact can have lower electron conductivity compared to the pristine graphene if the flakes are not completely reduced. In conclusion, all the methods reported need further developments in order to obtain low cost, high quality, reliable and scalable graphene and to be part of a production line.

## 2.2 Experimental Session: Synthesis of the Graphene

One of the main goals of this section is to explore different graphene synthesis methods and compare them in terms of efficiency, yield and quality of the graphene sheets produced. The approaches investigated were chosen in order to satisfy the constraints of safety, low cost, easy manufacturing, and high yield for large scale production. The most common methods have been also investigated like the Hummer's method introducing a microwave treatment in to shorten the time of the reaction, but no satisfying results have been obtained, because the process resulted to be too aggressive and the particles size was reduced to few nanometers, introducing many defects. Electrochemical exfoliation has been also investigated but it was discarded as the previous method because it was not considered a green route for the graphene production due to the use of acidic solutions and because the defect introduced in the resulting product after the oxidation and the reduction processes.

The methods presented in the next sections, have been chosen instead in order to avoid potential hazardous materials, high temperatures processes and toxic reducing agents, preferring more environmentally friendly and safer material and processes. Direct exfoliation methods have been employed as a green route for the graphene production, avoiding toxic and corrosive materials and using simple processes for the production of few layer graphene sheets from graphite powders. By only using of exfoliation methods, it is possible to avoid oxidation and subsequently reduction processes that, as was explained above, are usually a source of defects and vacancies in the atomic structure of the graphene, bringing to a deficit of performance of the final product. The direct exfoliation processes investigated are also considered fast, low cost and favorable to possible scaling up into a production level. In figure 2.3, are illustrated the process steps of an exfoliation process, with the intercalation of a chemical species (molecules, ions, etc.), into the graphite layers, first to weaken up the Van der Waals forces that keep the layers together and then second and last step of the sonication in a solvent, that helps the actual exfoliation of the graphite through a mechanical shearing effect.

The two processes that are presented in the next sections involve the exfoliation of the expanded graphite in different solvent. The expanded graphite was purchased from Asbury

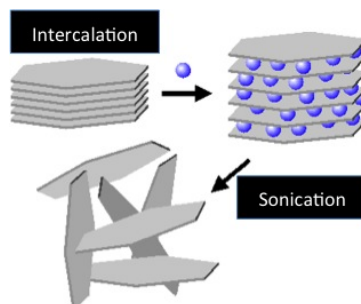


Figure 2.3 Representation of the intercalation/sonication process used to exfoliate the Graphite.

Carbons and it is a type of graphite that has been processed by a thermal expansion method, that produce the characteristic "worm-like" shape which is possible to observe in the Scanning Electron Microscope (SEM) pictures showed in Figure 2.4. This structure is created from the synthesis process that this graphite is subjected to; in fact, it is synthesized by the intercalation of compounds that expand when heated creating the exfoliated shape. A wide variety of chemical species have been used to intercalate graphite materials. These include halogens, alkali metals, sulfate, nitrate, various organic acids, aluminum chloride, ferric chloride, other metal halides, arsenic sulfide, thallium sulfide, etc. and if the graphite is exposed to a rapid increase in temperature, these intercalation compounds decompose into gaseous products, which results in high inter-graphene layer pressure. This pressure develops enough force to push apart graphite basal planes in the z axis direction. The result is an increase in the volume of the graphite and in an increase of the surface area as put in evidence in Figure 2.4 in the high magnification picture, showing the graphite layers separated forming a porous like structure.

Raman spectroscopy has been performed on the commercial starting material (expanded graphite) and its spectrum is reported in Figure 2.5.

Raman spectroscopy is a method largely used for the characterization of the graphene and, its use helps in the detection of the number of layers, disorder, doping level and all these parameters they can be detected by a short time measurement in ambient condition avoiding serious degradation of the graphene. The standard measurement data analysis consists in collecting the spectrum of the material and by subtracting it from the spectrum of the substrate (generally a silicon wafer). The highest peak present in a Raman spectrum of the graphene is the G peak about  $1580\text{ cm}^{-1}$  and then the 2D peak



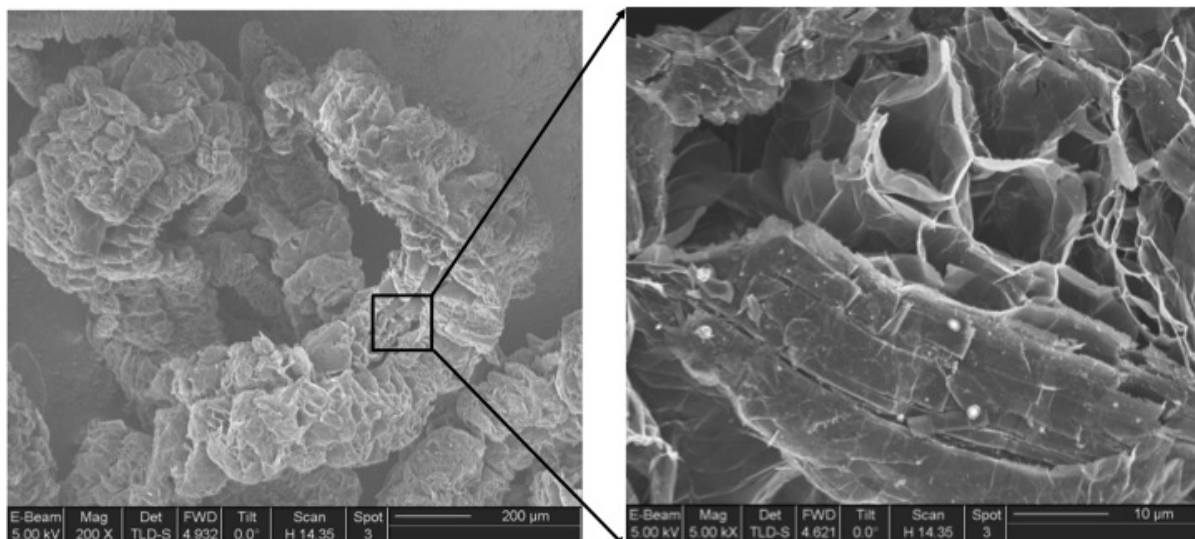


Figure 2.4 SEM pictures of Expanded Graphite flakes.

at  $2700\text{ cm}^{-1}$  another peak usually present is called D peak at  $1300\text{ cm}^{-1}$  that represent the amount of disorder of the material and it is usually not present in highly oriented pyrolytic graphite. In Figure 2.5 the highest peak showed in a Raman spectra is the G peak at about  $1579\text{ cm}^{-1}$  while the smaller one is the 2D peak positioned at  $2718\text{ cm}^{-1}$  [ref 65]. The graphitic nature of the expanded graphite has been verified also with the X-Ray diffraction technique (XRD), that as shown in Figure 2.6, presents a sharp peak around  $26.4$  degree d space  $0.34\text{ nm}$  that is typical for graphitic materials.

This type of graphite has been chosen as starting material for the experimental synthesis of the graphene because of its larger interlayer distance, as previously explained, considered an advantage for the intercalation/exfoliation processes for the production of few layer graphene. The exfoliation methods compared in this dissertation have been performed using different solvents and, in the next sections, all the results obtained from the characterizations will be reported.

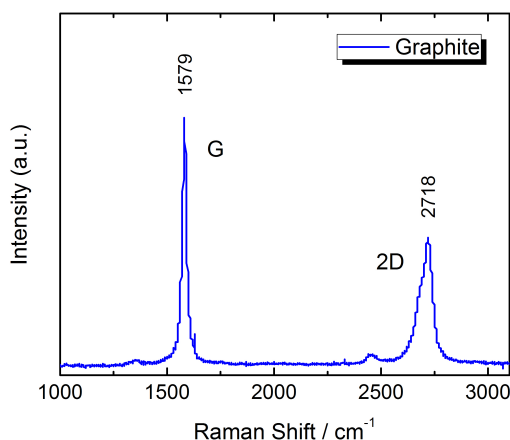


Figure 2.5 Raman spectroscopy spectrum of the Expanded Graphite.

### 2.2.1 Synthesis of Few Layer Graphene in N-Methyl-2-Pyrrolidone

Liquid chemical exfoliation of graphite oxide is now one of the most widely used methods for preparation of graphene. This method begins with intercalation of graphite with strong oxidizing agents followed by expansion of graphite layers via sonication. The reduction of the obtained graphene oxide to graphene is usually conducted by either thermal or chemical approaches (53), (64). Although this method is capable of high-yield (>50%) production of graphene, the use of large quantity of acid and oxidizing agents requires time-consuming washing steps and produces hazardous wastes. In addition, the vigorous oxidation of graphite often leads to incomplete restoration of the sp<sup>2</sup> hybrid carbon bonds and presence of residual oxygen functional groups resulting in poor electrical conductance (8). As an alternative way, exfoliation of natural graphite flakes into graphene in various solvents by sonication has been reported (54), (55), (65) and (66). This method represents a simple and direct processing to produce graphene sheets free of defects or oxidation that other approaches suffer. The graphene sheets can be dispersed in a small number of solvents that allowed the dispersion to be stable and the exfoliation to occur because of the strong interaction between the solvent and the graphite flakes that energetically make the exfoliation favorable and the subsequent solvation. The successful exfoliation relies on the proper choice of special solvents, such as N-methylpyrrolidone, which exhibit a surface energy matching to that of graphene and thus are capable of provid-

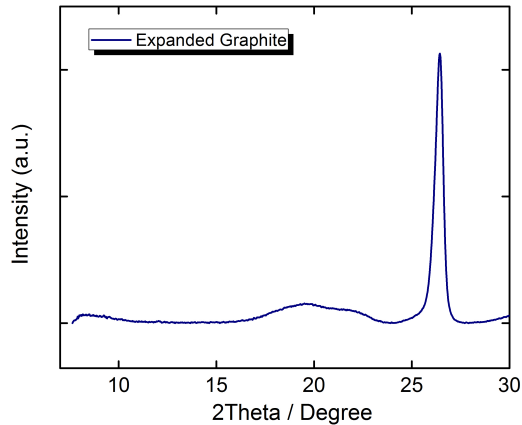


Figure 2.6 X-Ray Diffraction spectrum of the Expanded Graphite.

ing sufficient solvent-graphene interaction to balance the energy cost for expansion of graphite layers.

Liquid phase exfoliation of natural graphite is easy to implement and can avoid the oxidation step of graphene. This method involves ultrasonic treatment of graphite in solvents such as N-methyl-2-pyrrolidone (NMP), NN-dimethylformamide (DMF), and -butyrolactone (GBL) (54). Among all the solvents, NMP gives the highest graphene yield due to its surface energy approaching that of graphite that is sufficient to overcome the interacting forces between graphene layers. Although it is similar to the liquid-phase exfoliation of graphite oxide, this method is unique with the absence of oxidative intercalation steps. Graphene prepared by this method was demonstrated to have low number of defects and oxygen functional groups. However, the yield is usually very low (about 1 wt%) because only the layers on the surface of the graphite were peeled off during sonication. Other approaches has been proposed by simple sonication in N-methyl-pyrrolidone (54), in that case the oxidation process was avoided but the yield was about 1%. Higher yield, about 3% was obtained using water/surfactant solution (55) and also exfoliating the expanded graphite in DMF (66). The approach that is presented in the next paragraphs consists of the direct exfoliation of expanded graphite in NMP without the introduction of surfactants.

### 2.2.1.1 Materials and Methods

The samples were prepared starting with a simple dispersion of 3 mg of expanded graphite purchased from Asbury Carbon, added in 3 ml of N-methyl-pyrrolidone (NMP) purchased from Sigma Aldrich. The dispersions were then treated with a ultra sonication process using a Branson 250 disruptor sonifier with a power of 200 W at the amplitude of 60% for 1 hour, shown in Figure 2.7. After the sonication process the samples were then centrifuged at 10000 rpm for



Figure 2.7 Pictures of the Ultrasonication tool used for the exfoliation of the expanded graphite flakes.

30 minutes in order to remove largest aggregates at the bottom of the vial. The supernatant part was finally washed with DI water trough filtration processes. In order to perform the characterizations with the field-emission scanning electron microscopy (FE-SEM), the samples were drop cast on a copper-carbon transmission electron microscopy grid, while for atomic force microscopy (AFM) and for Raman spectroscopy analysis the samples were prepared by spin coating on top of a clean silicon wafer.

### 2.2.1.2 Results and Discussion

Morphological characterizations of the product obtained from the exfoliation method in NMP have been performed, and in Figure 2.8 AFM and FE-SEM pictures are reported, showing the presence of flakes of few layer graphene obtained from the process described above.

As it is possible to notice the size of the flakes is really small, with a diameter of about 1  $\mu\text{m}$ . The graphite flakes are not completely exfoliated, as shown in the FE-SEM picture,

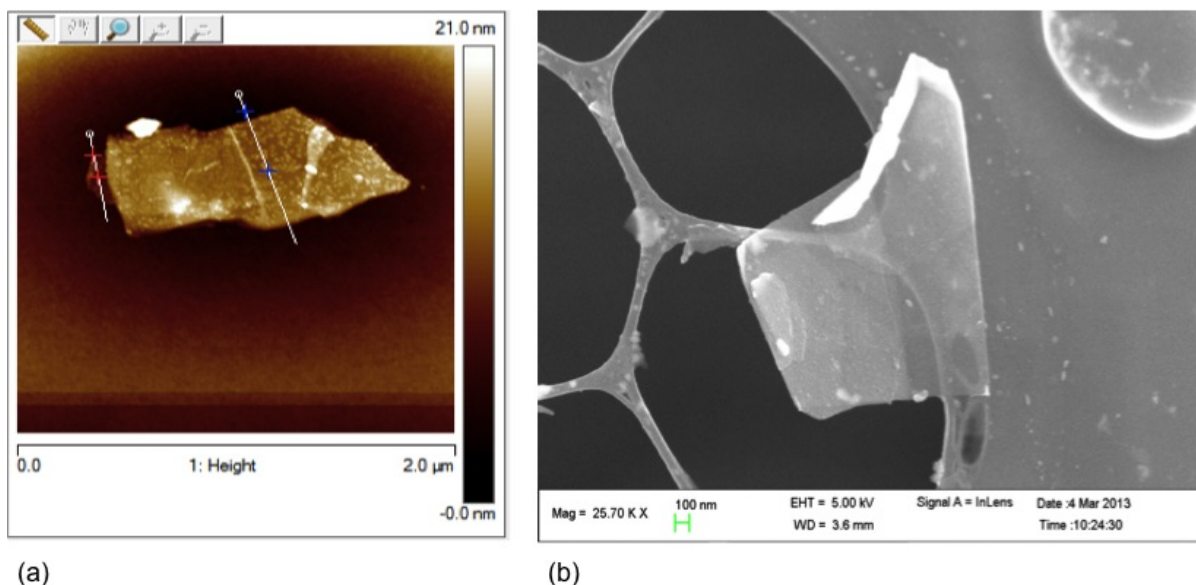


Figure 2.8 AFM picture (a) and SEM picture (b) of few layer graphene exfoliated in NMP.

and several layers are still present, reducing the transparency of the flakes. This observation is also confirmed by profilometry measurements performed with the AFM software program Nanoscope Analysis of the Veeco Instruments, showed in Figure 2.9. By analyzing two regions of the same flakes, different high values have been obtained, respectively 9.2 and 4.2 nm, that correspond to different numbers of layers.

Raman spectroscopy has been also performed as a compositional characterization to confirm the nature of the flakes. It is possible to notice in Figure 2.10 the appearance of the D peak

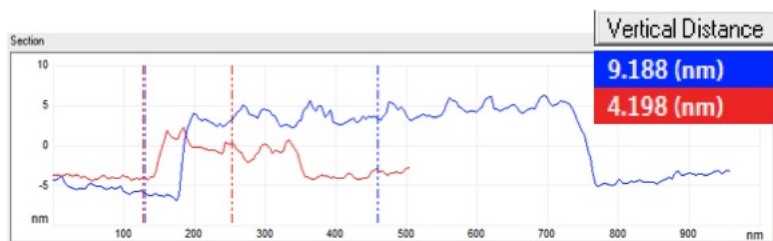


Figure 2.9 AFM height profiles of few layer graphene exfoliated in NMP.

at  $1349\text{ cm}^{-1}$ , that represents the amount of disorder of the material; the shapes of the peaks have been analyzed and compared to the Raman spectrum of the starting material showed in

Figure 2.5 and it is possible to see that the position and the shape of the 2D peak it is still really similar to the starting material meaning that the graphite has not been exfoliated enough.

In conclusion, this methods has reached a yield not higher than 3%, the size of the flakes

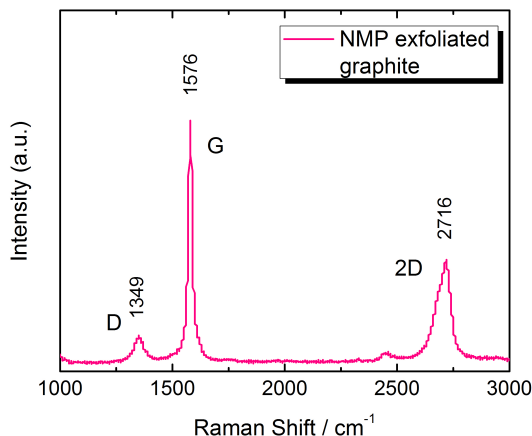


Figure 2.10 Raman spectrum of few layer graphene exfoliated in NMP.

resulted really small, more like a particle size of about 1  $\mu\text{m}$  and the dispersions resulted not stable in time, as precipitates were visible after only few hours.

### 2.2.2 Synthesis of Few Layer Graphene in Ionic Liquids

Direct liquid-phase exfoliation offers several advantages, the resulting colloidal suspensions of graphene are still at low concentrations as showed in the previous paragraph, therefore alternative liquid-phase processes, capable of producing a reasonably high concentration of stable graphene suspension, are highly desirable. The key parameters for such a process are the properties of solvents used. In this section is presented the work done in order to develop an easy and effective method to obtain few layer graphene sheets through the direct exfoliation of expanded graphite in ionic liquids. Ionic liquids are organic or partially inorganic salts, and are liquid at temperature below 100°C (67), (68). They are used in several alternative synthetic approaches (69) including those related to the green chemistry (70), because of some of their properties, such as compatibility with a wide range of organic and inorganic solvents, extremely

low vapor pressures, good thermal stability and no-inflammability (71). The ionic liquids are also recyclable and can be easily separated from other materials by liquid/liquid extraction (i.e. distillation) or solid phase extraction (i.e. ionic exchange).

Ionic liquids have surface tensions (74) closely matching the surface energy of graphite, which is a key prerequisite of solvents for direct exfoliation of graphite (54) and it has also been reported the possibility of exfoliate graphite powder in ionic liquids creating high concentrations up to 0.95 mg/ml (75), (76).

The basic structural attribute of ionic liquids is their ionicity, a unique feature favorable for stabilization of exfoliated graphene via Coulombic interaction through image charges (77), (78), such advantages over most solvents (54) that make ionic liquids the ideal systems for synthesis of graphene. It has already been observed, that the imidazolium-based ionic liquids can be successfully used as solvents for untangling carbon nanotubes (72), and the explanation stands in an interactions between p electrons of the nanotube and the positive charge of the imidazolium ring. Therefore, imidazolium based ionic liquids have been successfully used as dispersants and stabilizers. Afterwards, it has been also reported that graphene nanosheets have been prepared by electrochemical synthesis in imidazolium base ionic liquids (52) and it has been reported that the ionic liquid 1-butyl-3-methylimidazolium hexafluorophosphate worked as a solvent to disperse graphene (73). In literature is also reported the use of imidazole base molecules in order to intercalate the graphite and consequently to weak the bonds, helping the final exfoliation of the graphite (81) and imidazolium salt have been employed for stabilize the graphene solution (82). On top of this reasons the ionic liquid they could give another component of mechanical exfoliation due to their viscosity value.

In this section will be presented the formulation of stable graphene dispersions in ionic liquids without any chemical modification or any stabilizing additive starting from expanded graphite. The choice of using expanded graphite instead of graphite powders has been made because there has to be a strong interaction between the solvent and the graphite flakes, in order to have an energetically favorable exfoliation and the subsequent solvation. In the case of the expanded graphite, the ionic liquids can penetrate in between the separated layers in a much easier way by obtaining larger graphene sheets and avoiding intense damages, by reducing the

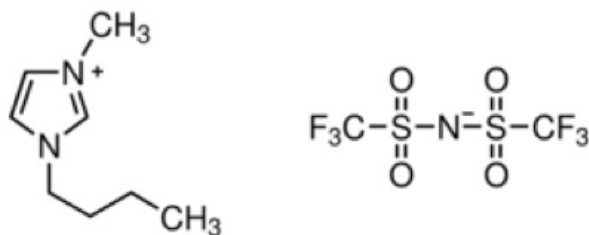


Figure 2.11 Pictures of the chemical representation of BDIM-TFSI (Ionic liquid).

exposure time under ultrasonic conditions.

### 2.2.2.1 Materials and Methods

Samples were prepared by using commercially available reagents. Expanded graphite was purchased from Asbury Carbon and used without further purification. Ionic liquids, dichloroethane, and isopropyl alcohol were purchased from Sigma-Aldrich. The Ionic liquids look like transparent solutions with a viscosity higher than water. In Figure 2.11 is reported the representation of one of the ionic liquid used for the exfoliation process. The cation group is the BDMI and the anion group is the TFSI with a polarity ET (30) of 48.6 kcal/mol (80).

The first step was the introduction of the expanded graphite flakes in 3 ml of Ionic liquids with a concentration of 1 mg/ml, and as it possible to see Figure 2.13 a, the graphite would stay at the top surface of the ionic liquid solutions due to the surface tension, respectively from left to right are showed 1-Butyl-2,3-dimethylimidazolium bis (tri- fluoromethylsulfonyl) imide (BDMI-TFSI), 1-butyl-3-methylpyrrolidinium bis (tri sulfonyl) imide (BMP-TFSI ), Ethyl-dimethyl- propylammonium bis (triimide (Solarpur), and 1-Ethyl-3-methylimidazolium dicyanamide (EMIM-DCA). The dispersions were then subjected to tip ultrasonication for a total of 30 min using 5-10 min on/off cycles (Branson 250 disruptor sonifier, 200 W) with an amplitude of power of 60%. The samples were then centrifuged at 15000 rpm for 20 minutes. The supernatant that looked still very homogeneous was then separated from the larger particles of graphite that deposited at the bottom of the vial.

In order to prepare the samples for the characterizations and confirm if few layer graphene was



produced, the material obtained from the exfoliation process was deposited on silicon wafers, after mixing 0.5 ml of DI water and 0.5 ml of 1,2-Dichloroethene (DCE) in order to create a separation of phase between the two solvents and isolate the graphene (83), (84) and adding to them 0.1 ml of the Ionic liquid/graphene dispersion. As it is shown in Figure 2.12 a "Meniscus" of graphene was obtained at the interface between DCE and water, making the transfer of the graphene on a substrate very straight forward. The silicon wafer that was chosen was a 300

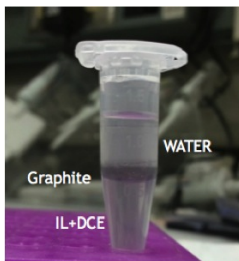


Figure 2.12 Pictures showing the separation of phase and the graphite located at the interface.

nm thermal oxide silicon wafer, the graphene was transferred on the substrate still sitting at the interface between water and DCE and the transferred on a hot plate to let the solvents evaporate and finally rinsed several times with ethanol and then dried using compressed air.

### 2.2.2.2 Results and Discussion

Imidazolium base ionic liquids as 1-Butyl-2,3-dimethylimidazolium bis (triimide (BDMI-TFSI), have surface tensions closely matching the surface energy of graphitic layer and interact non-covalently with the conjugated graphitic surface through and/or cation stacking. During the sonication treatment the graphite was subject to the exfoliation process, that occurred by mechanical shearing in the viscous solutions; at the end of the treatment the dispersions looked much darker due to the dispersed graphite flakes, homogeneously dispersed and very stable, showing very small levels of sedimentation as it is possible to see in Figure 2.13 b.

Several characterizations have been performed in order to investigate the morphological and compositional properties of the final product obtained through the sonication process. Field-emission scanning electron microscopy (FE-SEM), atomic force microscopy (AFM) and optical

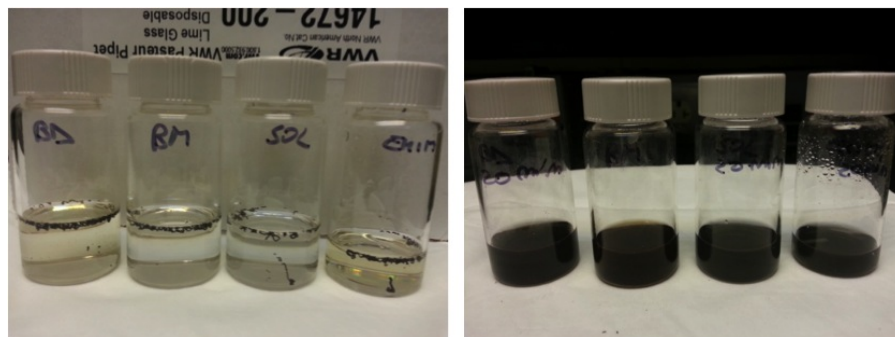


Figure 2.13 Pictures of (a) the Ionic liquids and (b) Graphite dispersions in Ionic liquids after sonication process.

microscope were used for morphological characterization and Raman Spectroscopy was also used for compositional characterization and in order to investigate the number of layer of the exfoliated graphite. After purifying and depositing the material on the silicon substrate, as described in the material and methods section, FE-SEM was performed as a preliminary investigation of the morphology of the few layer graphene obtained. Comparing Figure 2.14 to Figure 2.4 it is clear to notice that the performance of the exfoliation process it is really efficient and that it produces flakes with similar thickness and slightly different shapes with a diameter in a range of 2-5  $\mu\text{m}$ . The FE-SEM pictures show the presence of few layers graphene on the silicon wafer, and the magnification in Figure 2.14 shows clearly a flake composed by few layers of graphene composed by five graphene layers. From the FE-SEM pictures it is also possible to notice that there is not a complete uniformity in the size and thickness of the few layer graphene flakes. This observation has been confirmed by the optical images of the sample deposited on the silicon wafer as showed in Figure 2.15.

The different colors in the optical picture are obtained because of the thickness of 300 nm of the oxide on top of the silicon wafer and they are directly related to the difference in thickness of the graphene flakes due to different refraction of the light. In order to obtain a more quantitative analysis by directly measuring the thickness of the flakes and comparing them, atomic force microscopy (AFM) analysis was also performed. The thickness of the few layer graphene was carried out by tapping mode AFM on samples prepared, like for the FE-SEM, by depositing the "meniscus" of material, obtained at the separation of phase of water and DCE,

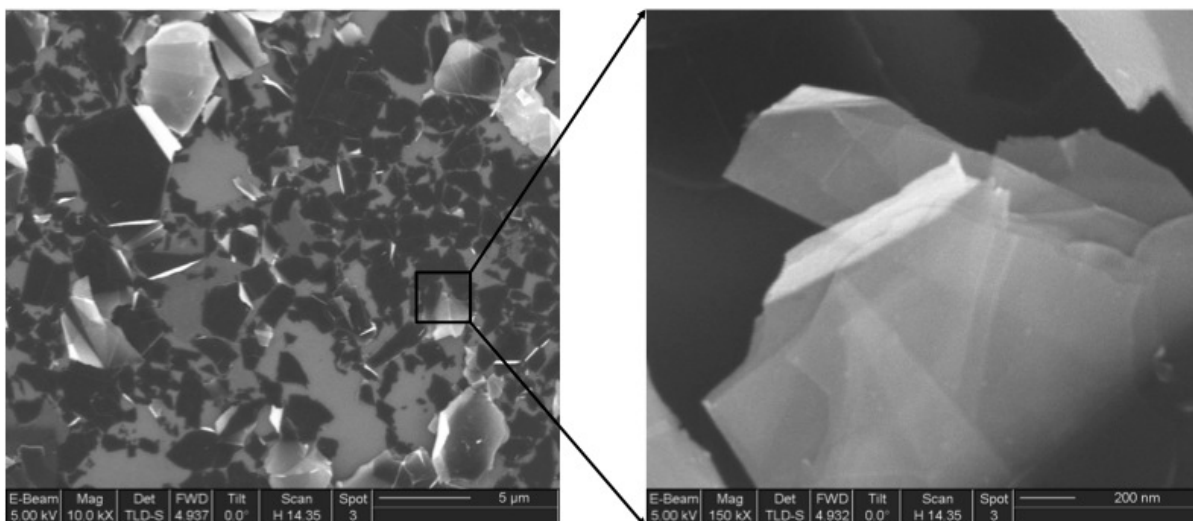


Figure 2.14 SEM pictures of the few layer graphene obtained from the exfoliation in ionic liquid.

on a silicon wafer. An AFM image of the deposited film is reported in Figure 2.16. The area scanned is of  $2.56 \mu\text{m}^2$ , the choice of this such small area was made in order to avoid thick residues not completely exfoliated.

The AFM analysis confirms the observation already made for the FE-SEM images, about the distribution in thickness and size of the flakes, and it was also confirmed by the profilometry analysis performed using the AFM software program Nanoscope Analysis from Veeco Instruments. In Figure 2.17 are shown profiles of three different flakes with a thickness of 4.2, 8.2 and 3.9 nm, respectively. It is possible to infer that the average thickness of the flakes is around 6 nm, showing a very big improvement compare to the starting material thickness and confirming the hypothesis that few layers graphene can be produced with the sonication of expanded graphite in ionic liquids.

The successful exfoliation of graphite into graphene flakes and the degree of exfoliation were further verified by Raman spectroscopy. As reported in the Appendix, Raman spectroscopy is a compositional characterization that can help in the estimation of the number of the layers of the exfoliated graphite, by analyzing the shape of the 2D peak, has reported by Ferrari et al. (63). This methods is applicable in particular when we are in presence of less than ten layers.

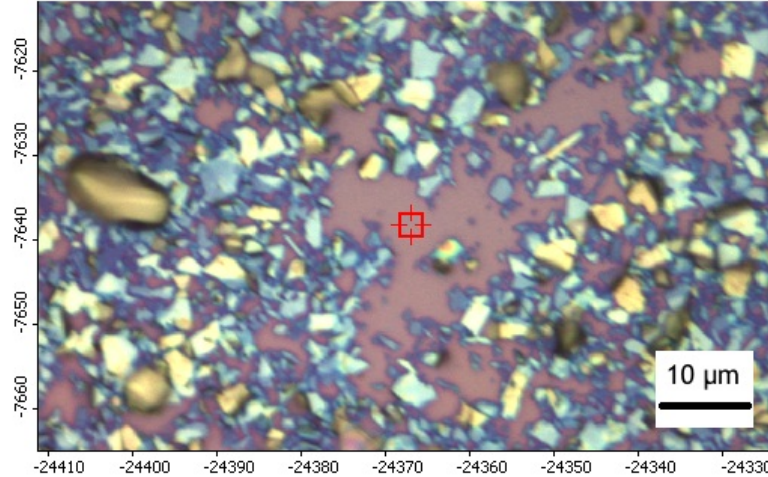


Figure 2.15 Optical microscope image on 300 nm SiO<sub>2</sub> wafer.

The exfoliated monolayer of graphene presents a symmetric and sharp 2D peak while, for few layer graphene the 2D peak usually is broader and asymmetric with a shoulder. Comparing the Raman spectra of the starting material (expanded graphite), showed in Figure 2.5 and the Raman spectra obtained from the product of the exfoliation process it is possible to notice some differences that are put in evidence in Figure 2.18, where three different samples: graphite (green curve), few layer graphene obtained from the ionic liquid exfoliation process (blue curve) and the commercial graphene sample (red curve) are compared. It is possible to see the appearance of a new peak around  $1350\text{ cm}^{-1}$ , the D peak, called also disorder related peak, that was not present in the expanded graphite (85). The D peak is mediated by an elastic scattering with defects and inelastic scattering with a phonon, and so it brings information related to the structure of the material and the amount of defects present in it. This appearance is a sign of the effect that the exfoliation process has on the material and in particular how the mechanical shearing and chaotic movement in the dispersion during the sonication process, can reduce the sized of the flakes and increasing defect on the surface and edges, but the high intensity ratio of  $I_G/I_D$  it reveals also that low levels of defects are induced by the exfoliation.

At the same time another effect of the exfoliation process can be observed in the Raman spectra, and it is the shift of the 2D peak towards smaller Raman shift. The effect it is showed in Figure 2.18, by comparing the relative position of the three 2D peaks of the three samples,

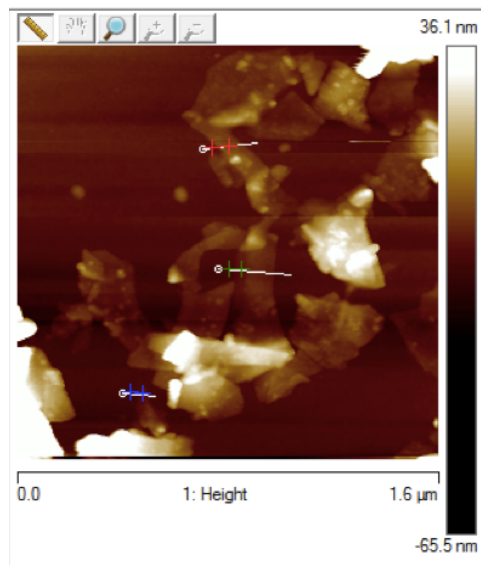


Figure 2.16 AFM Height scan showing the few layer graphene obtained by ionic liquid exfoliation.

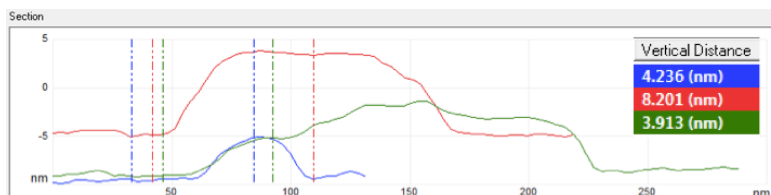


Figure 2.17 AFM profile measurement showing the different thickness of the few layer graphene flakes.

that shows a shift from  $2715\text{ cm}^{-1}$  of the expanded graphite to  $2703\text{ cm}^{-1}$  of the exfoliated few layer graphene to  $2675\text{ cm}^{-1}$  of the commercial graphene.

A modification of the shape towards a more symmetric and sharp peak typical of the graphene can also be seen. This effect it is observable in the Raman spectra reported in Figure 2.19 in which the 2D peak of the exfoliated sample is losing its asymmetry and shifting to  $2705\text{ cm}^{-1}$  (86), if compared to the asymmetric shape with a shoulder typical of the graphitic materials (see Figure 2.5).

The 2D peak of the carbon materials is mediated by two inelastic scatterings and it is more sensitive to the electronic structure of the graphene and its analysis is possible to distinguish a monolayer from a few layer graphene analyzing the 2D peak as Ferrari's group reported, see

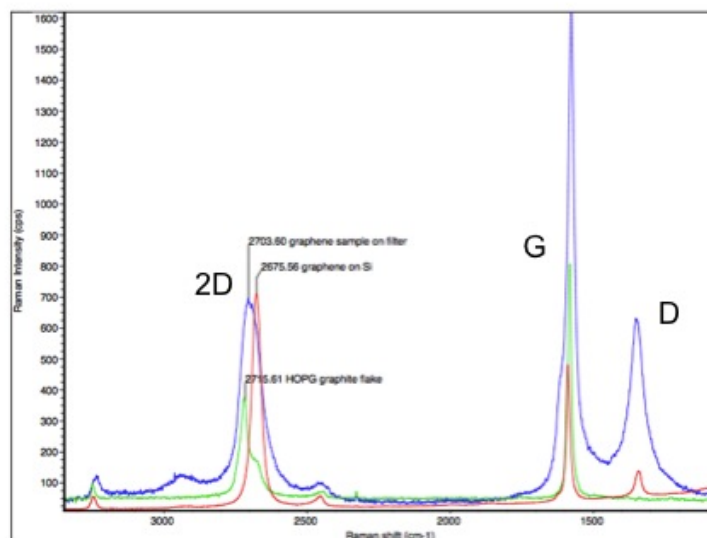


Figure 2.18 Raman spectroscopy spectrum showing the shift of the 2D peak after the exfoliation process of the Expanded Graphite (green)  $2717\text{ cm}^{-1}$  and two samples (blue and red)  $2703$  and  $2675\text{ cm}^{-1}$ .

Figure 2.20 (63).

In order to understand in which region belonged and how many layers were composed of the product coming from the exfoliation in ionic liquid, the 2D peaks were analyzed, and two representative peaks are reported in Figure 2.21. By comparison with the peaks reported in Figure 2.20 it is possible to confirm that the shape of the 2D peaks of the ionic liquid-assisted exfoliated graphene resembles to the ones previously reported for thin flakes and that the flakes obtained consist in about two and five monolayers, confirming the results previously observed by other characterizations.

Preliminary impedance measurements have been also performed on three different dispersions in order to evaluate electrical conductivity properties of ionic liquid formulations with carbon fillers. BDMI-TFSI ionic liquid itself, BDMI-TFSI with exfoliated expanded graphite and BDMI-TFSI with commercially available graphene were prepared following the same procedure explained in the material and methods section. In order to analyze the electrical properties the samples were assembled in coin cells filled with the three dispersions and the

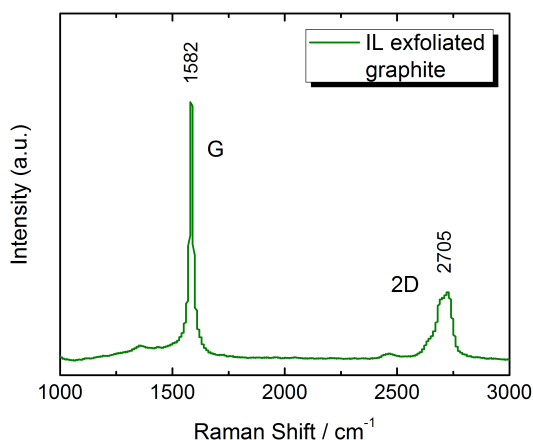


Figure 2.19 Raman spectroscopy spectrum of the Expanded Graphite after the exfoliation process.

EIS setup, showed in Figure 2.22, was then used for the impedance characterization.

The results are reported in Figure 2.23. It has been observed an improvement in the impedance values trend in the formulation with carbon filler compared to the impedance of the ionic liquid itself and that the sample with exfoliated expanded graphite is almost comparable to the one obtained by dispersing commercial single layer graphene in the ionic liquid.

### 2.3 Conclusion

In summary, it was demonstrated that few layer graphene can be prepared using direct exfoliation by sonication of expanded graphite in ionic liquids solutions. The suitable surface tensions and ionic feature facilitate the exfoliation of graphite and the imidazolium based ionic liquid helps the stabilization of the few layer graphene also in presence of a high concentration of suspension. This methods can be considered a simple and green method that avoids oxidation and subsequent reduction steps for the synthesis of few layer graphene. It has been proved that by using direct exfoliation of the expanded graphite in ionic liquid solutions by sonication process, few layer graphene flakes can be obtained, characterized by a number of layers that ranges between 2 and 5 and particles diameter of about 4  $\mu\text{m}$ .

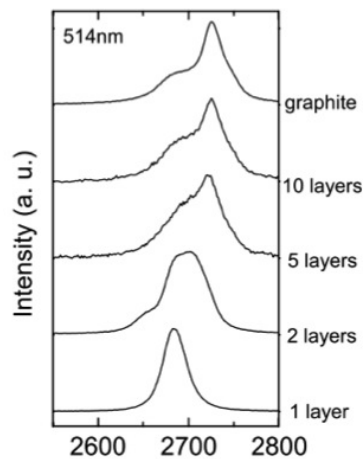


Figure 2.20 Raman Spectrum of Graphene and Graphene Layers A. C. Ferrari, J. C. Meyer, V. Scardaci, C. Casiraghi, M. Lazzeri, F. Mauri, S. Piscanec, D. Jiang, K. S. Novoselov, S. Roth, and A. K. Geim, *Phys. Rev. Lett.*, 2007, 97, 187401.

It is possible to conclude that this process can be considered as a possible environmentally friendly, simple and fast method for the exfoliation of the graphite and the synthesis of few layer graphene.



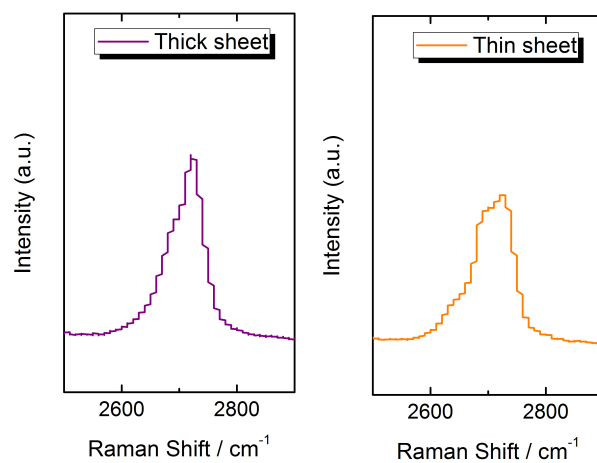


Figure 2.21 Raman spectroscopy spectrum of the 2D peak of two Expanded Graphite flakes with different thickness.

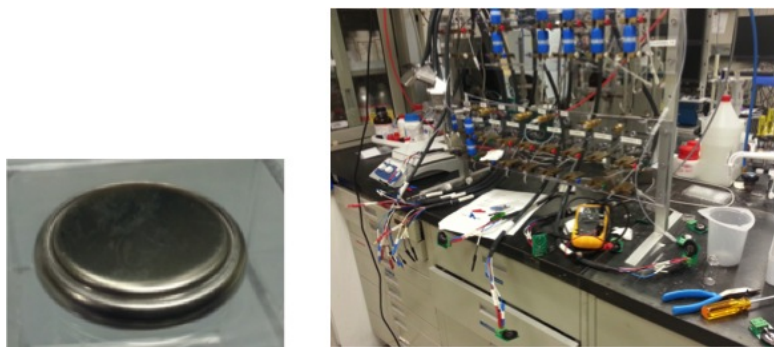


Figure 2.22 Coin cell on the left used for impedance measurements and impedance setup.